JOURNAL OF GEOPHYSICAL RESEARCH, VOL. 103, NO. D12, PAGES 13,763–13,775, JUNE 27, 1998

Breakup of levitated frost particles

Neil J. Bacon
Physics Program, University of Washington, Seattle, Washington

Brian D. Swanson and Marcia B. Baker
Geophysics Program, University of Washington, Seattle, Washington

E. James Davis
Department of Chemical Engineering, University of Washington, Seattle, Washington

Abstract. We have studied the sublimation and breakup of single 100–200 μm frost particles levitated electrically at temperatures in the range $-2°C$ to $-30°C$. Breakup rates were largely independent of temperature and humidity in this range but strongly dependent on particle shape. Irregular particles of high aspect ratio were most likely to break up. Sublimation (evaporation) was accompanied by an increasing aspect ratio. A linearized sublimation model, presented in the appendix, accounts for the observation that thin neck regions were not subject to enhanced sublimation rates. Estimates of the forces involved in breakup suggest that the breaking strength of these frost particles is considerably less than that of bulk ice. We discuss possible implications of our results for ice particle multiplication in clouds.

1. Introduction

1.1. Ice particle breakup and cloud microphysics

The concentration of ice crystals in clouds often exceeds that of ice-forming nuclei by a substantial margin [e.g., *Hobbs and Rangno,* 1990; *Blyth and Latham,* 1993], and there have been a number of attempts to define the mechanism(s) responsible for the ice particle enhancement. Among these are fragmentation during ice-ice collisions [e.g., *Griggs and Choularton,* 1986], heterogeneous freezing and shattering of supercooled raindrops [e.g., *Hobbs and Alkezweeny,* 1967], splintering during riming of small graupel pellets, known as the Hallett-Mossop (HM) process [e.g., *Hallett and Mossop,* 1974], and ice particle breakup during sublimation [*Oraltay and Hallett,* 1989]. In recent analyses of field observations from cumuliform clouds [*Hobbs and Rangno,* 1990; *Blyth and Latham,* 1993], the presence of very high concentrations (in the range 1–1000 per liter) of small ice particles at cloud-top temperatures warmer than about $-20°C$ was found to be explainable in most, but not all, cases in terms of the HM process. This mechanism is active under a highly constrained set of thermodynamic and microphysical conditions [*Mossop,* 1978] and its efficiency is influenced by cloud dynamics [*Blyth and Latham,* 1997]. *Bower et al.* [1996] report several observations of extremely high ice particle concentrations at temperatures near $-15°C$, a temperature at which dendritic crystals are common and the HM process is ineffective. Although it is possible that splinters produced by the HM process at, say, $-8°C$ are advected up to the $-15°C$ level, it seems likely that we need to invoke other mechanisms for multiplication to explain the observations. Moreover, *Rangno and Hobbs* [1991] estimated that the glaciation they observed was an order of magnitude faster than could be accounted for by the HM process alone. It therefore is of interest to examine the simplest possible ice multiplication mechanism; namely, breakup of complex ice particles, which may operate over different ranges of the relevant parameters.

Paper number 98JD01162.
0148-0227/98/98JD-01162$09.00

1.2. Previous Experiments and Motivation for This Work

Previous authors have studied the breakup of ice particles grown on substrates. *Schaeffer and Cheng* [1971] observed that whiskers were ejected from frost during growth, while some authors have linked the breaking off of frost particles to the positive charging that has been observed during growth [*Rydock and Williams,* 1991; *Saunders et al.*, 1993; Y.Y. Dong and J. Hallett, preprint, 1990]. *Oraltay and Hallett* [1989] observed breakup of millimeter-scale dendrites mechanically suspended in a diffusion chamber at temperatures near the melting point, with wind speed chosen to emulate fall velocities. They observed breakup at low relative hu-

midities and at high temperatures but not at relative humidities (with respect to ice) > 70% for ice-bulb temperatures below −3°C.

Because of the need for substrates in these experiments, the mechanics of the breakup could not be studied with sufficient detail to estimate the breaking strength of the particles, needed for eventual prediction of the role of breakup in clouds. The levitation of ice particles in our electrodynamic balance eliminates the need for a substrate and allows observation of single particles over periods of up to several hours (depending on the growth or sublimation rate). Thermal and epitaxial effects of the substrate can be avoided and atmospheric conditions can be closely mimicked, although the following differences should be noted:

1. The particles carry charge and experience electric fields that are not always present in the atmosphere. Electric fields are known to modify growth rates of ice particles at ambient field strengths of 5×10^4 V/m [*Bartlett et al.*, 1963; *Crowther and Saunders,* 1973], about an order of magnitude stronger than the fields in our chamber. *Crowther and Saunders* [1973] found that needle-like ice crystals were affected but hexagonal plates were not, suggesting that field enhancement at tips may be important. The effect on sublimation rates is not known, but the rounded habits of sublimating particles are likely to minimize electrical effects. The effect of surface charge density associated with net charge is not known. In general, a change in overall sublimation rate in our experiment should not affect the likelihood of eventual breakup.

2. The particle motion is dissimilar to that of atmospheric particles. The current setup does not allow for airflow to simulate falling particles, in contrast to the experiments of *Oraltay and Hallett* [1989]. We presume that while ventilation would enhance the sublimation rate for a given undersaturation, the likelihood of eventual breakup would not be significantly altered. This remains an open question, the key point being whether the effect is different for different regions of the particle. The ventilation effect is likely to be small for particles of 100 μm scale. Such particles have fall speeds of order 0.1 m/s [*Jayaweera and Cottis,* 1969] and hence a Reynold's number of about 0.5, leading to a ventilation coefficient of less than 1.1 [*Pruppacher and Klett,* 1978].

We chose to study frost particles partly because of the ease of introduction into the balance and also because they are expected to behave similarly to both dendritic particles in clouds and frost grown on graupel. The goals of our experiments were the following:(1) to explore the ambient conditions and particle shape characteristics leading to breakup, (2) to measure the shape evolution of sublimating particles, and to compare with predictions based on a simplified model, and (3) to estimate the breaking strength of small frost particles. In addition to these experimental goals, we also set out to estimate the relative importance of breakup during sublimation to cloud glaciation.

2. Experimental Procedure

2.1. Apparatus

The apparatus consisted of an electrodynamic balance with an internally mounted diffusion chamber, shown schematically in Figure 1. The chamber was 4 cm in height and 5 cm in diameter; the circular walls were made of PVC, while the top and bottom endcaps (A and B) were copper. The upper vapor source consisted of filter paper wetted with deionized water and attached to the underside of the upper endcap. The lower vapor source was a sheet of ice frozen from deionized water on the lower endcap. The apparatus was located inside a cold room that controlled the overall temperature, while a heater (C) and a thermoelectric cooler (D) gave thermal control over the upper and lower endcaps, respectively. More details are given by *Swanson et al.* [1998]. Temporal variations in the wall and endcap temperatures of up to 0.5°C were attributable to the cycling of the cold-room thermostat and other external factors; variations in the temperature difference between the endcaps were an order of magnitude smaller.

A dc potential difference of 0–700 V was applied between the endcap electrodes, providing a field from 0– 5

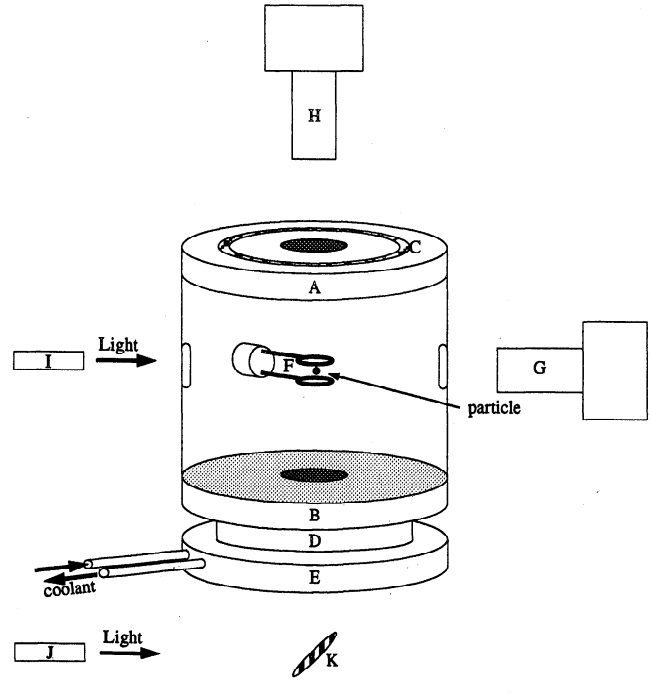

Figure 1. A schematic of the apparatus. A dc potential difference is applied between the copper endcaps (A and B), which hold the vapor sources. An electrical heater (C) heats the upper endcap, while a thermoelectric cooler (D) attached to a heat exchanger (E) cools the lower endcap. An ac potential applied to the rings (F) stabilizes the particle at the center of the balance. Light sources (I and J) provide backlighting for the video telemicroscopes (G and H), which view the particle through windows. The mirror (K) deflects the beam upward through a window in the lower endcap.

kVm^{-1} at the center of the balance to levitate charged particles. An ac potential applied to a pair of concentric rings (F) confined the particle to a localized orbit that in most cases was smaller than the particle size. The concentric ring design was chosen to allow unobstructed viewing of the particle from the top and sides. The dc voltage and the ac voltage and frequency were recorded continuously.

Video telemicroscopes (G and H) were positioned to obtain top and side views through glass windows, with back lighting provided by a dual-outlet halogen lamp (I and J) of adjustable intensity. This broadband lamp, modulated by an infrared filter-mirror combination, doubled as a heat source that made undersaturated conditions possible (see section 2.3.3). A mirror (K) was used to deflect a light beam through a small window in the bottom of the chamber for the vertical camera, while a direct beam was used for the horizontal camera. The light intensity controlled the shutter speed; image jitter could be eliminated by setting the ac frequency to a multiple of the video sampling frequency of 60 Hz.

2.2. Experimental Protocol

The chamber was cleaned daily with deionized water and every 2 weeks using isopropyl alcohol followed by deionized water. The supersaturated conditions in the diffusion chamber caused frost to grow overnight on the chamber walls and on the rings in the center. Before each experiment, the frost was removed from the walls, producing an assortment of frost particles at the bottom of the chamber. A hypodermic needle was used to "flick" frost particles up, causing a single particle to be trapped between the rings. The particles carried a net electrostatic charge with a typical magnitude in the range 0.1–0.5 pC; both signs of charges were seen, although most (about 80 %) were positive.

The dc voltage and ac frequency were adjusted to hold the particle steady at the center of the balance. Periodically, at intervals of about 2 min, the frequency was reduced until the onset of vertical instability in the orbit was reached, at which point the frequency and voltages were recorded; these data carry information on the particle size and charge (see section 2.3.2). The amplitude of the unstable oscillation was 500 μm or less, and the duration was at most 5 s. The error in the dc balance voltage and the ac frequency at instability are estimated to be 5%.

The temperature difference between the endcaps was set between 0°C and 15°C and the lamp intensity together with the infrared filter-mirror combination was used to control the conditions at the center of the balance. In general, with low intensity and with the filter-mirror in place, the particles grew, while sublimation could be achieved by removing the filter-mirror and increasing the light intensity. The dc voltage and ac frequency were continuously varied to keep the particle localized at the balance center, although it became difficult to stabilize particles smaller than 10–20 μm. For this reason, particles that sublimated down to this size were recorded as sublimation without breakup. A chromatographic anion analysis was performed on frost particles gathered in the balance, and the results are shown in Table 1.

Table 1. Results of a Chromatographic Anion Analysis of Frost Particles Collected in the Balance

Species	Concentration, ppmm
Organics	0.05
Cl^-	0.65
NO_2^-	0.03
NO_3^-	0.06
SO_4^{2-}	0.06

The chlorine concentration is comparable to that of rainwater, and concentrations of nitrates and sulfates are two orders of magnitude smaller than are found in rainwater [*Warneck*, 1988].

2.3. Measurements

2.3.1. Optical measurements. The magnification of the telemicroscopes could be varied over a sevenfold range, with a maximum on-screen magnification of approximately 1000. Most pictures were taken at intermediate magnifications. We monitored video images in real time and recorded them on VHS tape for later analysis. Frame-grabbing software ("NIH Image," available from the National Institute of Health) allowed images to be captured and analyzed. A diffraction grating was imaged in order to calibrate both the video monitor and the digital images at the various magnifications of the telemicroscopes; this calibration agreed to within 5% with images of a 20 μm polystyrene latex sphere that we trapped and imaged in the balance.

Linear dimensions and projected areas were measured digitally using the frame grabbing software to an accuracy of a few percent; in most cases the limiting factor was not the resolution of the camera but reorientation of the particle. Because of the irregular shapes of the particles, any realignment tended to create large uncertainties in size measurements. For this reason, accurate optical size analysis was possible only in the few cases where the particle orientation with respect to at least one of the cameras remained steady. The resolution limit at the highest magnification was of the order of 1 μm. All of the linear dimensions reported in this paper were measured optically, though it is also possible to infer an equivalent linear dimension using only the instability measurements [*Swanson et al.*, 1998].

2.3.2. Size and Charge Determination. In addition to the optical measurements, the voltages V_{ac} and V_{dc} and the frequency of orbital instability f can

be used to obtain the mass, charge, and equivalent radius r_{eq} of the particle (the radius of a sphere of equal volume). Briefly, the levitating voltage gives the charge-to-mass ratio of the particle, while a second relationship is obtained from the instability measurement, given the approximation that particle behaves dynamically like a sphere of equal volume. Details of this analysis are given by *Swanson et al.* [1998]. In our experiments particle sizes and linear dimensions were measured optically, and the instability data were used only to determine the charge, given by

$$q = -\frac{4\pi\rho g z_0 r_{eq}^3}{3C_0 V_{dc}}, \quad (1)$$

where ρ is the particle density, z_0 is the chamber height, and $C_0 = 0.69$ is a dimensionless constant set by the geometry of the balance. Because the equivalent radius r_{eq} is cubed in (1), an error in r_{eq} can produce a substantial error in q: up to 50% in the cases of rapid sublimation when there was not sufficient time for accurate instability measurements. We hope to improve on this in future work. We have no way to estimate the error in the density of irregular-shaped particles, for which determination of the volume of a particle is problematic. We used a value of $\rho = 910$ kg/m^3, which is an upper limit for frost; hence the charge we calculate should also be seen as an upper limit.

2.3.3. Temperature and relative humidity estimates. It was not possible to measure the temperature T and relative humidity at the center of the balance. Instead, a relaxation code was used to deduce a temperature and a vapor content at the center of the balance from the measured temperatures of the walls and the endcaps, assuming saturated ice/water conditions at the boundaries. Direct radiative heating of the particle did not appear to be the dominant cause of sublimation, although this may play a role. Also at play is the indirect heating due to absorption by the window, rings, and surrounding air, which raises the ambient temperature thereby causing sublimation under conditions that more closely resemble those in clouds. We estimated the role of direct and indirect heating effects by noting that they lead to distinct size versus time dependences. The glass window strongly absorbs at wavelengths longer than about 1.5 μm; ice is weakly absorbing in the range 0.6–1.5 μm. For sublimation due only to this weak absorption, the direct heating rate scales with the particle volume, leading to an exponential decay of the equivalent radius, which was not observed. The shapes of the inferred radius versus time graphs indicate that indirect heating was the dominant mechanism of sublimation: We found that by adding an offset to the center temperature, the sublimation data could be fit with a simple model of vapor and (latent) heat diffusion. When the lamp was turned to full power without a heat filter, an offset of 1.2°C fit the data well throughout the temperature range of our observations.

3. Results

3.1. Conditions Leading to Breakup

We observed no breakup during the growth of 30 frost particles grown at rates ranging from 0.005 to 0.15 μm/s. We saw frost particles break up during sublimation on numerous occasions, and the results are summarized in Table 2, which shows the bulk average properties of particles that broke up and those that did not. The sublimation rates ranged from 0.005 to 1.7 μm/s.

Particles that broke up tended to be aggregate or irregular in character, and in all such cases, the original particle had a neck region that was thinner than adjacent sections. Figure 2 shows some of the particles that eventually fractured. Those shown in Figures 2a and 2b display irregular dendritic features. In Figures 2c and 2f the neck region is located in the middle of the particle, while in Figures 2d and 2e it separates a relatively small feature from the main body of the particle. In a minority of cases (Figure 2c is one such example), the particles developed elongated necks connecting bulbous features at the ends. Pristine columnar or platelike crystals did not break up: Particles that broke tended to be prolate with an aspect ratio of three or more. Breakup of oblate particles was rare and occurred only when a small feature broke off (see, e.g., Figure 2e) or when the particle was aggregate in character (such as two plates apparently sintered together).

Figure 3a shows all of the sublimation events according to the initial size and aspect ratio: Particles that broke up are shown as triangles and are concentrated at higher aspect ratios on the prolate side of the abscissa. Breakup was most probable for large (> 100

Table 2. Summary of Particle Properties

	Number of Events	Average Initial Size, μm	Average Final Size, μm	Average Temperature, °C	Average Charge(pC)
Sublimation with breakup	44	163 ± 79	126 ± 72	-9.4 ± 7.0	0.29
Sublimation without breakup	76	104 ± 49	13±7	-8.0 ± 5.5	0.29

The particles are separated into those that broke up and those that did not. The size given corresponds to the maximal dimension of the particles and is reported with standard deviation. Particles that broke up were on average larger than those that did not. No significant difference in average temperature or charge on the particles is found.

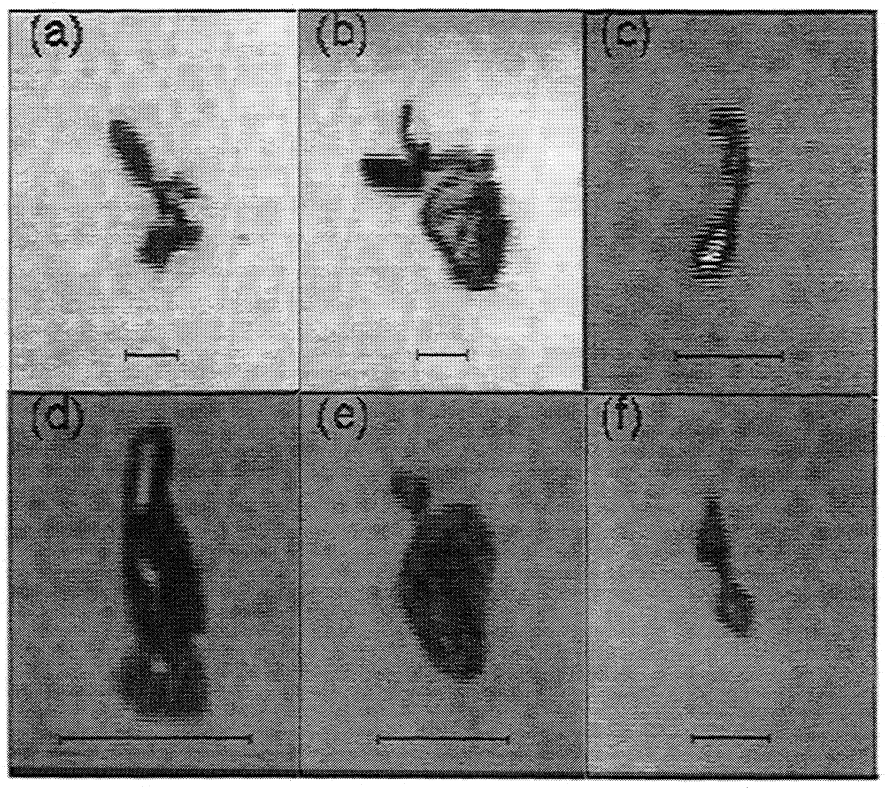

Figure 2. Some typical frost particles that later broke up. The scale shown in each frame is 100 μm long.

μm) particles, perhaps because of the fact that irregular dendritic particles tended to be large (see Figures 2a and 2b); these were the particles most predisposed to break up. Figure 3b shows relative humidity versus temperature for the same events. No discernible dependence of the breakup rate on temperature is evident from this plot: On the contrary, a breakup rate of 1 in 3 is maintained throughout the temperature range (though there are fewer data points at lower temperatures). It is evident from this plot that we observed breakup in the region in which *Oraltay and Hallett* [1989] reported that dendrites of millimeter scale did not break up during sublimation: relative humidity with respect to ice $RH_i > 70\%$ and ice-bulb temperature $T_i < -3°C$ (i.e., the range of actual temperatures extends to temperatures warmer than $-3°C$, depend-

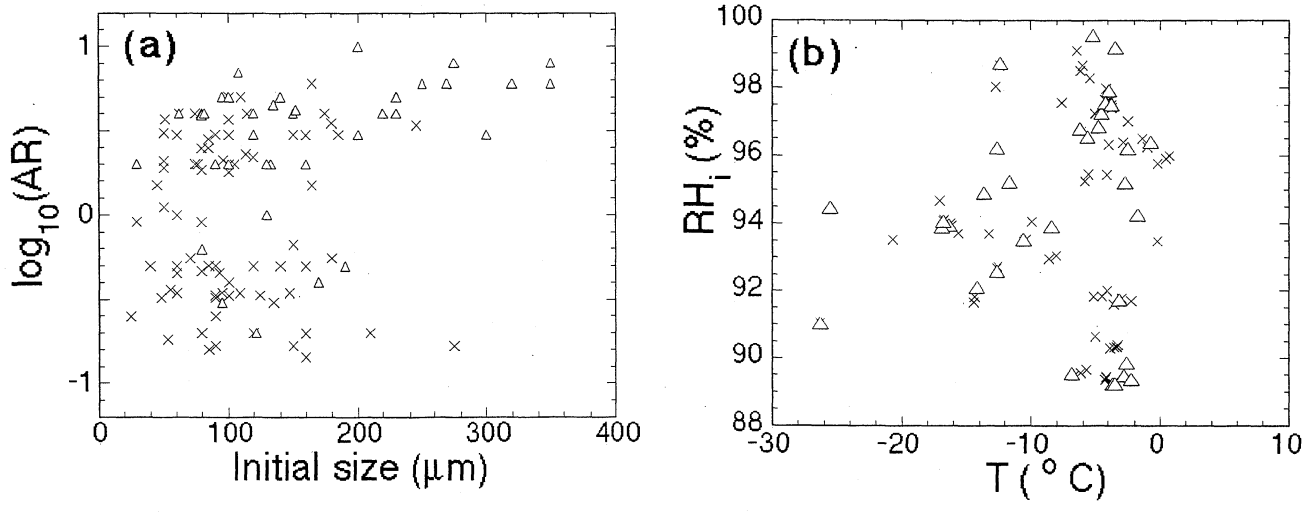

Figure 3. Sublimation with breakup (triangles) and without breakup (crosses). (a) Logarithm of the initial aspect ratio Γ plotted against initial size (maximal dimension): $\log \Gamma > 1$ corresponds to prolate particles and $\log \Gamma < 1$ corresponds to oblate particles, and (b) relative humidity (over ice) versus temperature.

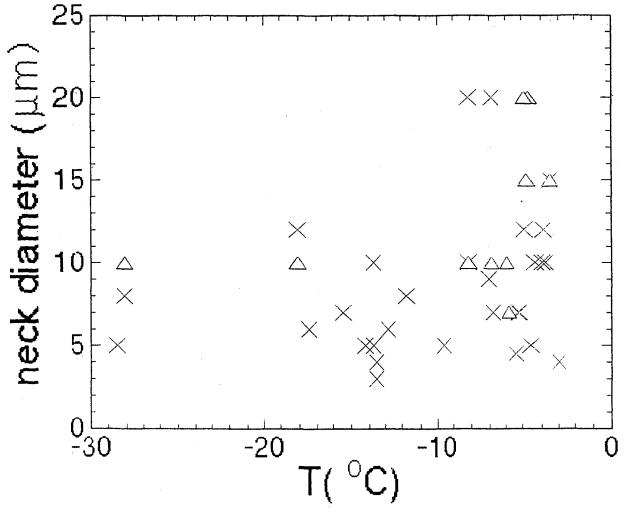

Figure 4. Neck diameter versus temperature for particles that broke up. Particles that reoriented prior to breaking up are shown as triangles.

ing on the humidity). Our results do not indicate any dependence of the breakup rate on relative humidity. Of the 44 breakup events, only one or two took place during an instability measurement, indicating that the accelerating forces did not play a significant role in the breakup process (see section 4).

Analysis of digitized images allowed measurement of the diameter of the neck the instant before it broke. In cases where an accurate measurement was possible, the diameter was found to be between 4 and 10 μm. In some cases, prior to breakup, the two fragments of the particle were observed to twist, rotate, or generally reorient relative to each other. Breakup usually followed a few seconds later but in some cases occurred a few minutes after the reorientation. This was particularly common at the higher temperatures, though a momentary twisting immediately before breakup was seen at -18°C and at -28°C . Figure 4 shows the neck diameter and temperature for all the breakup events. Particles that reoriented prior to breakup appear as triangles; they are seen to be concentrated at higher temperatures.

During the course of the experiment, the opposite of breakup, sintering, was seen on 5 occasions. This occurred as a result of a second particle falling into the balance, presumably from the walls or the rings. Apparently, the two particles were of opposite charge as they were observed to attract one another. This hypothesis is supported by the inferred charge on the particle, which decreased at the sintering event (see Figure 5). In one case, the sintered pair was observed to separate after a period of sublimation.

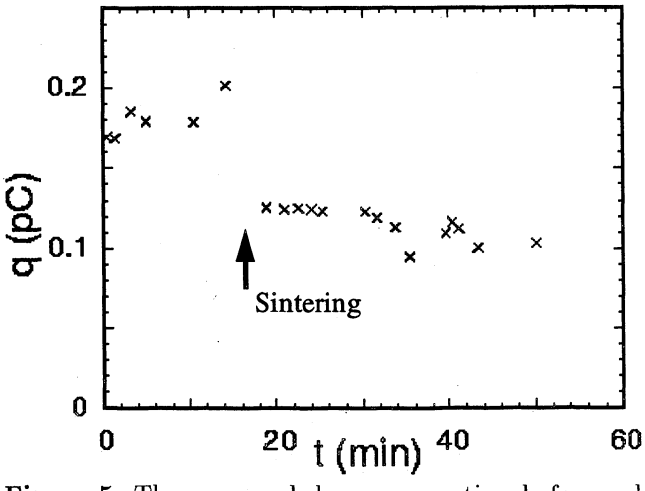

Figure 5. The measured charge versus time before and after sintering, at $t = 16$ min. The drop in charge implies that the particle that fell in was charged oppositely (though not equally) to the original particle.

3.2. Optical Analysis

When it was possible to make reliable measurements, the length, neck diameter, and, if appropriate, the dimensions of other features on the particle were measured. Figure 6 shows a schematic view of a particle for

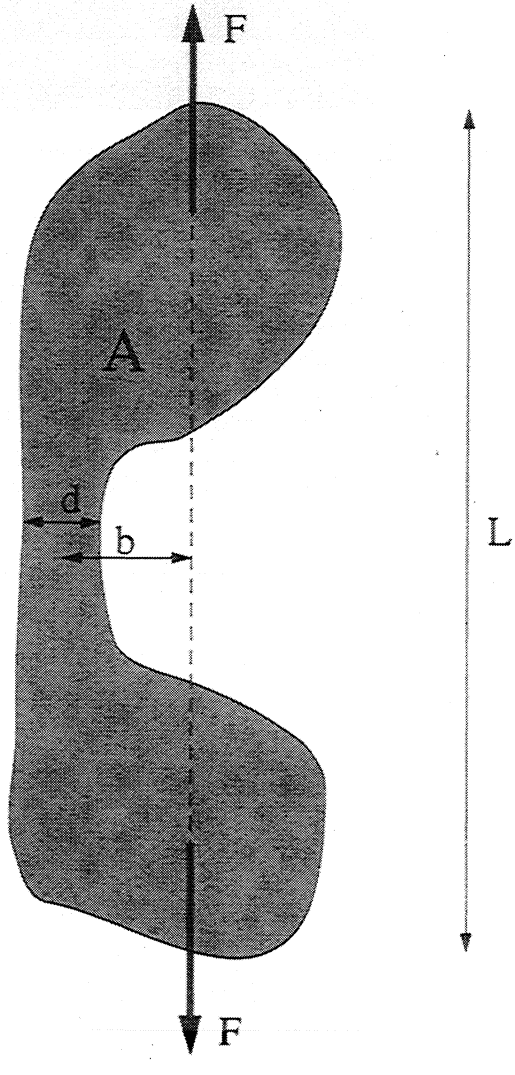

Figure 6. Sketch of an irregular particle, showing the various dimensions that were measured: length L, projected area A, and off-axis distance b, the distance between the center of the neck and the axis along which the net repulsive force F acts.

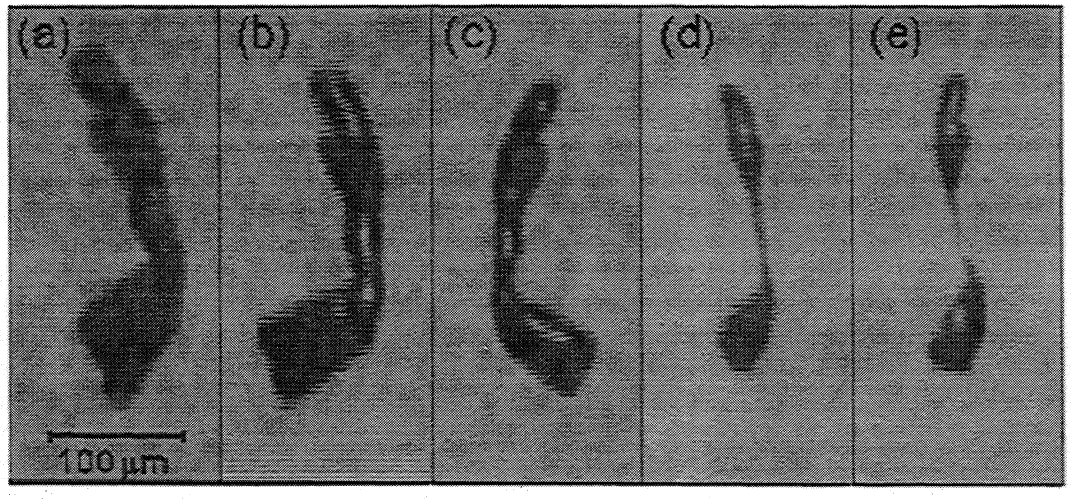

Figure 7. A frost particle that broke up, shown at (a) 6 min before breakup, (b) 4 min before breakup, (c) 2 min before breakup, (d) 20 s before breakup, and (e) at the moment of breakup. The length L and the diameters of the upper and lower protuberances d_1 and d_2 and that of the neck region d_3 were measured optically. Note the development of a long neck.

which one could measure a length L, a projected area A, and lateral diameters. The parameter b is discussed later in section 4.2. If the particle approximates a solid of revolution, then these measurements are more meaningful; care was taken to choose particles that came close to this criterion (particles tended to align vertically, and the image from the vertical camera gave an indication of rotational asymmetry). We were able to deduce a characteristic aspect ratio Γ from the length L and area A shown schematically in Figure 6 by

$$\Gamma = L^2/A. \tag{2}$$

Figure 7 shows one of the particles for which optical measurements were made, at various stages during its evolution from 6 min before breakup in Figure 7a to the instant of breakup in Figure 7e. Notice how the relatively narrow midsection seen in Figure 7a develops into an extremely thin neck, just a few micrometers across in Fig 7e. The diameters of the upper and lower protuberances, respectively d_1 and d_2, and that of the neck region d_3 were measured optically. We could evaluate Γ from measurement of the overall length L and projected area A. The results of these measurements are shown in Figure 8. Note that the 3 diameters change at rather similar rates, while the length changes more quickly but not fast enough to keep the aspect ratio (indicated by the solid line) constant. Further discussion of sublimation is given in section 4.4.

4. Discussion

4.1. The Mechanism of Breakup

In order to estimate the breaking strength of the frost particles, we now consider the various forces that might act to break up a frost particle levitated in our balance and try to give estimates for each. We shall argue that Coulomb self-repulsion is the dominant force that causes breakup in our experiment, and we will use our estimates of this force to derive a breaking strength for frost. We consider this force to be important in our experiment but not central to the breakup of particles in general, since continued sublimation would no doubt lead to breakup in the absence of this mechanism.

4.1.1. Induced charge. The electric fields in the balance give rise to an induced dipole moment on a particle, leading to a mechanical tension within the particle (the two ends of the dipole experience opposite forces in the ambient field). For an ice particle of permittivity $\epsilon_r \approx 100$ in an initially uniform electric field $E_0 \approx 10^4$ V/m along its axis, we calculate the polarization charge on the surface to be of the order of 10^{-15} C for a sphere of diameter 100 μm and less for prolate ellipsoids of the same length [see, e.g., *Jackson*, 1975; *Bartlett et al.*,

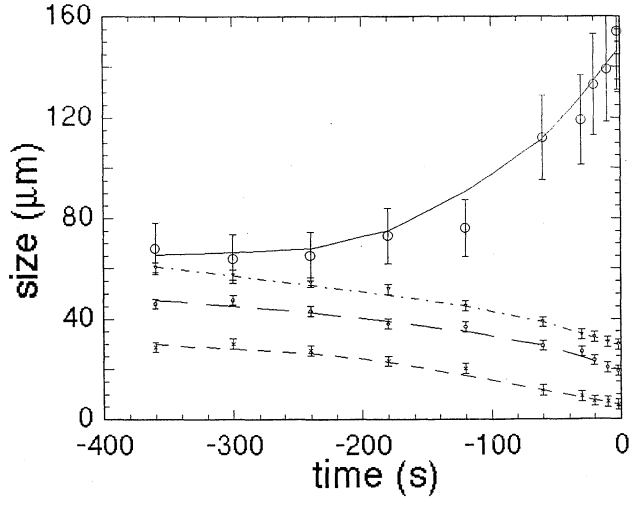

Figure 8. Dimensions of the particle shown in Figure 7 as a function of time: d_1 (long dashes), d_2 (dash-dotted), and d_3 (short dashes), with the aspect ratio Γ ($\times 10$ μm) fitted with a solid line.

1963]. The forces associated with these charges are of the order of 10^{-12} N, and are not significant compared with other forces described below.

4.1.2. Differential drag. The drag force acting on a particular section of a particle will not in general scale with the mass of that section, resulting in a tension or compression within the particle. To estimate the magnitude of this force, we consider an idealized particle made up of two spheres of radii a_1 and a_2 connected by a thin bridge. We consider motion along the axis of the particle, and from the Stokesian drag acting on each sphere (the drag on the bridge section is neglected), we calculate the tension in the connecting section as

$$T = 6\pi\eta v[(a_2 a_1^3 - a_1 a_2^3)/(a_1^3 + a_2^3)], \qquad (3)$$

where η is the dynamical viscosity and v is the velocity. In the limit $a_1 \gg a_2$, this tension approaches $6\pi\eta a_2 v$. The maximal velocity of the particles in this experiment, occurring in the instability tests, is $\sim$ 0.1 m/s, giving a differential drag of approximately 10^{-10} N for $a_2 = 10$ μm (note that the Reynold's number is less than 1 even in this maximal case). Although the model used here is crude, we believe that the order of magnitude of the result is correct and that we are justified in ignoring this force in our calculations. This contention is supported by the fact that only a small minority of particles actually broke up during an induced orbital instability (where the velocity and hence the drag forces are maximal). This force may play a role in the breakup of actual cloud particles.

4.1.3. Nonuniform charge distribution. We can estimate the effect of nonuniform distribution of charge on the particle surfaces by consideration of an extreme case as follows: If all of the charge is on one half of the crystal and all the mass on the other, then the tension due to gravitational and electric fields is just the weight of the particle. In this limiting case, the force is roughly 10^{-10} N for a 100 μm particle. A similar contribution comes from the accelerating forces during an orbital instability: the maximum acceleration is $\sim 10g$, so we can expect a tension of at most 10^{-9} N due to this motion. As noted above, only one or two particles actually broke up during an instability measurement, so forces of this magnitude are not significant in this context.

4.1.4. Field nonuniformity. The force due to electric field nonuniformity can be estimated using the results of a relaxation method computation of the fields inside the balance. The vertical component E_z of the peak ac field evaluated along a vertical line through the center of the balance was calculated, and the gradient of this component at the center was found to be $dE_z/dz \approx 4 \times 10^7$ V/m^2. Thus over a 100 μm particle, the change in field is $\delta E_z \approx 4 \times 10^3$ V/m. For particles carrying the charges we inferred ($10^{-13} - 10^{-12}$ C) this leads to a tension/compression force of about 10^{-9} N.

4.1.5. Coulomb self-repulsion. In order to estimate the magnitude of the electrostatic repulsive force of the charges on the particle surface, we considered the simplified case of a cylinder with equidistant charges on its surface to deduce the net repulsive force experienced by each half of the cylinder due to the charges on the other half. (*Andrews* [1997] suggests that this is not an unrealistic approximation for the charge distribution on a thin prolate object.) Using characteristic values of charge and particle dimensions for our particles, we found that this repulsive force was in the range $10^{-7} - 10^{-8}$ N (see Table 3), orders of magnitude larger than the other force estimates. Therefore we assume that this force is the most important for particle breakup in our experiment, and we use it to estimate the breaking strength of the ice particles.

4.2. Breaking Strength

In order to relate the force estimate to a breaking strength for the particles, we must consider the nonuniformity of stress due to bending moments on a particle. These arise because the net force acts off the axis of the neck region, generating a bending moment that must be counteracted by differential stress across the neck. For the particle shown in Figure 6, we can calculate the stress variation across the neck assuming the cross section to be a square with side d and that the force $\vec{F}$ acts off the axis at a distance b from the center of the

Table 3. Breaking Strength Estimate for Selected Particles

Length, μm	Aspect Ratio	q,pC	Neck Diameter d, μm	Coulomb Force, nN	Average Stress, bar	b/d Estimate	Breaking Strength, bar
101	8	+0.44	4	74	0.058	1.0	0.42
210	15	+0.45	6	24	0.008	2.0	0.11
250	7	-0.82	8	41	0.008	2.0	0.11
138	14	+0.63	4	105	0.084	0.5	0.34
130	5	+0.63	7	73	0.019	1.0	0.13

The data in the first three columns are used to derive the Coulomb force, as described in section 4.1.5. This force is used along with the measured neck diameter and off-axis parameter b/d to derive a breaking strength estimate (see (5)), shown in the last column. The values deduced are lower than that of bulk ice, which has a breaking strength of about 15 bars [*Hobbs*, 1974].

cross section. To the extent that the stress-strain relationship is linear, the stress varies linearly across the cross section, such that

$$\sigma(y) = \frac{F}{d^2} + \lambda y, \tag{4}$$

where λ is a constant (the ratio of Young's modulus to the bending radius) and y is the distance from the center of the cross section. Balancing forces and moments gives a maximum stress (occurring on the right-hand side of the neck in Figure 6) as

$$\sigma_{\max} = (F/d^2)[1 + 6(b/d)]. \tag{5}$$

We have identified this maximal stress with the breaking strength. A crack would be initiated at the point of highest stress and, once started, would propagate, since the effective cross section is decreased by the appearance of the crack. Using (5), we have estimated the breaking strength of several frost particles. The results are shown in Table 3. The Coulomb force F was calculated using the cylindrical model described in section 4.1.5, and the off-axis parameter b/d was estimated optically (see Figure 6).

Experimental studies on the breaking strength of ice reveal strong dependence on both sample size and shape. *Jellinek* [1958] reported that the breaking strength increases with decreasing sample volume but diminishes with decreasing cross-sectional surface area, an effect he attributed to the statistical effects of imperfections that will propagate a crack only a limited distance. He attempted to parameterize these effects, and although the cross-sectional areas he studied were 0.2 cm^2 and higher, one can attempt to extrapolate his results to smaller cross-sectional areas. His results imply a limiting value for the breaking strength of between 5 and 15 bar as the cross sectional area approaches zero. *Hobbs* [1974] reviewed experimental studies on the breaking strength of ice, citing values in the range of 10–20 bar in the appropriate temperature range. Our estimates shown in Table 3 are 2 orders of magnitude lower than these. It is noteworthy that *Bartlett et al.* [1963] also deduced a small breaking strength (order of 10^{-3} bar) for millimeter-scale frost dendrites. Two possibilities are that either frost is generally much weaker than bulk ice or the strength decreases dramatically at small scales, in line with Jellinek's hypothesis. In his paper Jellinek commented that the bulk strength of ice is much less than the theoretical strength one gets by setting $S = 2\gamma/x$, where γ is the surface free energy density and x is the distance over which the work of rupture must take place. (He estimated $x \approx 2 \times 10^{-8}$ cm, $\gamma \approx 76$ erg/cm^2 and deduced a theoretical strength of 7600 bar.) He concluded that imperfections play an important role in the breaking of ice. This is in agreement with earlier, more general, studies of brittle fracture [*Inglis,* 1913; *Griffiths,* 1920; see also *Lawn,* 1975] in which the effect of imperfections and stress concentrators was taken into account. Cavities in the frost may act as stress concentrators in the manner described by *Lawn* [1975].

4.3. Effect of Impurities

The concentrations of chlorine ions shown in Table 1 are comparable to those found in rainwater, and those of sulfates and nitrates are about 2 orders of magnitude smaller [*Warneck,* 1988]. We do not have information on contamination of atmospheric ice particles with which to compare our data nor on levels of organics in atmospheric ice or rain. It should be noted that the contamination levels we report apply to frost particles gathered in the balance over a 2 week period, and do not necessarily correspond to the levels in the actual frost particles that we studied. Our analysis did not test for the presence of ammonia or CO_2, both ubiquitous in the laboratory and both associated with the weakening of ice at high concentrations (in excess of 3 ppmm)[*Mossop,* 1980; *Nakamura and Jones,* 1973]. We were unable to investigate the effects of impurity concentration in grain boundaries and effects of incorporated air on the plasticity of the ice.

4.4. Plastic Deformation as a Breakup Mechanism

Previous studies of polycrystalline ice [*Jellinek,* 1958; *Dempsey,* 1996] and of soft hail [*Dong et al.*, 1994] have found an increase in strength at small scales for 0.1 to 100 cm pieces of ice (although Jellinek reported that the strength decreases with decreasing cross-sectional area). Our measurements of low strength for small (0.01 cm) particles suggest that different mechanisms may operate at this scale or that the method for preparing the ice sample has a large influence on the strength of the ice.

The breakup strengths we report were derived by treating the breakup process as brittle fracture. For some particles we observe what appears to be plastic deformation prior to breakup (see section 3.1). An example of this is shown in Figure 7e, where a kink in the narrow bridge section appeared 0.15 s prior to breakup. The two segments then proceeded to twist relative to each other before breaking. This process is reminiscent of the deformation of single ice crystals observed by *Glen and Perutz* [1954] and by *Readings and Bartlett* [1968], raising the possibility that similar mechanisms may be at work. In single-crystal regions of a particle where the c axis is not parallel to the applied stress, resolved shear can cause macroscopic sliding along the basal plane, thus contributing to the low breaking strength. In polycrystals, this sliding is inhibited by neighboring grains, whereas the neck regions of our particles may be single crystals. This possible difference in crystallinity may account for the anomalously low breaking strength of our particles. In support of this notion is the fact that the breaking strengths we derived are close to values for critical shear stress in the literature: *Readings and Bartlett* [1968] gave 0.2 bar as a critical shear stress for basal slip and *Steinemann* [1954] gave 0.2 bar for an

upper limit for basal shear strength (cf. our values in Table 3).

It should be added that we had no direct measure of the crystallinity of the particles. We suspect that the grains are at least 10 μm in extent, since particles of that scale usually grow (if we change the conditions in the chamber) with habits characteristic of single crystals, while larger-seed particles tend to develop complex polycrystalline habits.

4.5. Sublimation

A general characteristic of the sublimating particles throughout the temperature range (−2°C to −30°C) was the rounding of sharp features and edges, an effect attributable in part to high vapor flux in the vicinity of small-scale features. One might expect that the same process would lead to accelerated sublimation of relatively thin neck regions connecting larger segments and so increase the incidence of breakup. This was not supported by our data. In our experiments, there was no indication that neck regions of the particles sublimated faster than thicker parts. For the particle chosen in Figure 8, the neck radius changed at about the same rate as other lateral radii (within the experimental precision), and this was found to be the case for all five of the particles that were analyzed this way. In some cases, in fact, the neck sublimated at a lower rate than other large features. This result is in agreement with the linear perturbation analysis presented in the appendix, showing that perturbations in radius are likely to grow only if their length scales are large compared to the radius; we interpret this in terms of shadowing by the surrounding protuberances.

As discussed in section 3.1, we were able to measure aspect ratios of the sublimating particles and found that they increased, or at least did not decrease, with time for all of the (above-mentioned) sublimating particles over the measurement period (Figure 8 shows one example). Our results are in contrast with the capacitance model of crystal growth and sublimation, in which the aspect ratio is maintained as the overall size changes, according to $c = \Gamma a$, where c and a are the height and width of the particle, respectively, and Γ is the aspect ratio.

5. Application to the Atmosphere

In the experiments described here, the ice particles carried significant charge, and, according to our estimates, Coulomb self-repulsion was the dominant cause of breakup. In a cloud, the particles would not carry such high amounts of charge (except in thunderclouds); however, our graphs of neck diameter versus time strongly suggest that, had breakup not occurred at the electrostatic limit, in each case, the neck would have continued to sublimate, leading to breakup due to differential drag or simply loss of material. Extrapolation of Figure 8 indicates that the neck diameter would have reached zero about 1 min after the breakup event had the breakup not occurred.

Breakup of sublimating particles may lead to ice particle multiplication in clouds in situations (such as entrainment regions near a cloud top) where zones of undersaturation and supersaturation are in close proximity (100 μm particles would not survive a large-scale convective downdraft). The original particles might be vapor-grown crystals of irregular habit, common in regimes that favor dendritic growth, or they may be frost removed from the surface of graupel pellets by collision with ice particles, although *Jayaratne et al.* [1996] maintain that this process is unlikely to be a significant source of particles. In order that the particle concentration is not ultimately diminished by sublimation, these undersaturated zones must have lifetimes shorter than that of the sublimating particles τ_{sub}. The lifetime of a turbulent eddy of length scale L in a cloud of turbulent kinetic energy dissipation rate ϵ ($\mathrm{m}^2/\mathrm{s}^3$) is approximately $\tau_L \approx (L^2/\epsilon)^{1/3}$. Typical values in active cumulus clouds are $\epsilon \approx 10^{-3} - -10^{-4}$ $\mathrm{m}^2/\mathrm{s}^3$ [*Baker et al.*, 1984] so that for $L \approx 100$ m, $\tau_L \approx 100$–1000 s. If the period of a downdraft eddy exceeds τ_{sub}, then we can expect the particles and daughter particles to sublimate away. If the eddy lifetime τ_L is shorter than the sublimation time for the particles τ_{sub}, then the particles may break up but not disappear during a downdraft (since breakup is temporally probabilistic, while sublimation is systematic). The sublimation time τ_{sub} is set by the undersaturation in the downdraft and by the particle sizes; in our experiment the average time for particles to sublimate from approximately 150 to 10 μm was $\tau_{\mathrm{sub}} \approx 420$ s, and for particles that broke up, the average time per breakup was $\tau_b \approx 280$ s. The ratio of the number of breakup events to the total number of particles was $\beta \approx 0.4$. We can estimate the particle production rate R_b from this mechanism as $R_b \approx \beta n_i / 2\tau_b$, assuming that half of the particles are in an undersaturated downdraft at any one time. We can compare this with rates from other ice-enhancement mechanisms using values typical of midlatitude cumulus and cumulonimbus clouds [*Rangno and Hobbs*, 1991; *Harris-Hobbs and Cooper*, 1987; *Blyth and Latham*, 1993] for the concentrations and kernel factors: We estimate $R_{HM} \approx 1$ $\mathrm{m}^{-3}/\mathrm{s}$ from the HM process in regions where it operates and $R_{fs} \approx 10^{-3} n_i$ $\mathrm{m}^{-3}/\mathrm{s}$ from freeze shattering due to capture of ice particles by raindrops. Using our values of τ_b and β, we find that R_b is comparable with R_{HM} for $n_i \geq 1000$ m^{-3} (1 per liter), relatively late in the multiplication process. However, given appropriate cloud dynamics, it may be the dominant mechanism when droplet size distribution factors or low temperatures (i.e. if the graupel surface is colder than −8°C) render the HM process ineffective.

One possible field test of the mechanism we propose would be a comparison of ice particle concentrations measured at different points within a cloud. Higher concentrations in undersaturated downdrafts would support our hypothesis.

6. Conclusions

We have seen that frost particles break up during sublimation over the temperature range −30°C to 0°C at relative humidities (with respect to ice) $100\% > RH_i \geq 85\%$, and that the probability of breakup is a strong function of particle shape. We saw breakup in the range of parameters for which *Oraltay and Hallett* [1989], who studied larger particles, did not. Accelerated sublimation of neck regions was not observed, an effect that we have explained via a simple model. Estimates of the breaking strength indicate that the frost particles are much weaker than bulk ice, possibly owing to basal slip in single-crystal sections.

The process that we have observed could be important in cloud glaciation depending on the particle shapes that are grown. Since it is the irregular particles that are most likely to break up during sublimation, an interesting process to investigate would be the breakup of dendrites grown and sublimated in our balance, if possible with controlled airflow to simulate fallspeeds. The report by *Bower et al.* [1996] of a spike in ice particle concentration near −15°C, where dendritic growth is expected, provides motivation for further investigation.

Appendix: Sublimation of an Infinite Cylinder With Perturbations

A.1. Introduction

The rate of sublimation of an irregular particle varies with position on the particle according to local geometric factors, due to two separate mechanisms:

1. The Kelvin effect is the change in the equilibrium vapor pressure over curved surfaces: The vapor pressure is increased by convex curvature and reduced by concave curvature (for which the radius of curvature is negative) according to

$$e = e_0 \exp\left[\frac{\gamma s^3}{k_B T}\left(\frac{1}{r_1}+\frac{1}{r_2}\right)\right], \tag{A1}$$

where e_0 is the equilibrium vapor pressure over a flat surface, γ is the surface free energy, s is the intermolecular spacing, k_B is Boltzmann's constant, and r_1 and r_2 are the two radii of curvature [*Hobbs*, 1974]. In the case of ice $s \approx 3$ Å and $\gamma \approx 0.08$ J/m^2 (depending on the orientation), so even for radii of curvature of the order of 1 μm, the effect is only about a tenth of 1%. For the particles we studied, this effect does not modify the sublimation rates significantly.

2. Of greater import is the fact that the vapor density gradient near the surface (and hence the flux of vapor) is set by the particle dimension: For this reason, small crystals sublimate more quickly than larger crystals for given ambient conditions. In the case of a nonspherical particle, small-scale features such as necks may experience this effect, but the influence of surrounding features on the vapor field must also be considered.

To estimate the magnitude of the second effect, we consider a cylinder with slightly varying radius sublimating sufficiently slowly that we can ignore transients in the vapor field. We consider only the diffusion-controlled regime in which the number density of water molecules in the vapor n satisfies Laplace's equation $\nabla^2 n = 0$. The narrowing of a segment on our cylinder will tend to increase the gradient in vapor density at the surface and hence, at first glance, will tend to increase the flux of vapor away from the surface. We assume the temperature is uniform along the cylinder, a valid approximation for slow sublimation since the thermal time constant $\tau = \rho c a^2/K_{\text{th}}$ is of order 10^{-2} s for an ice particle of 100 μm scale (ρ is the density of ice, c is the specific heat, a is the particle size, and K_{th} is the thermal conductivity). In order to maintain the uniform equilibrium vapor pressure at the surface, the vapor field is perturbed with a decay length dependent upon the wavelength of the radius perturbation. The result, as we shall see, is that only perturbations of wavelength long compared with the cylinder radius are expected to grow.

A.2. Calculation

For simplicity, we consider an infinite cylinder of radius $R(z)$ sublimating in a vapor field that is bounded at radius b ($b \gg R$), where the vapor number density is fixed at some value n_b. Without perturbations, $R(z) = a$ and the unperturbed vapor field is

$$n(r, z) = n_0(r), \tag{A2}$$

where $n_0(r)$ is the solution to

$$\nabla^2 n_0(r) = 0, b \geq r \geq a \tag{A3}$$

subject to the boundary conditions

$$n_0(a) = n_a \tag{A4}$$
$$n_0(b) = n_b \tag{A5}$$

and has the form

$$n_0(r) = -\frac{n_a - n_b}{\ln(b/a)} \ln r + \text{const}, \tag{A6}$$

where n_a is the uniform equilibrium number density at the surface of the cylinder. Let the perturbed boundary of the cylinder be

$$R(z) = a + \zeta(z), \tag{A7}$$

where

$$\zeta(z) = \delta a \sin kz, \tag{A8}$$

and $\delta \ll 1$. In order to maintain the boundary condition $n(R) = n_0(a)$ at the perturbed boundary, a second term must be added to the vapor field. To first order in δ,

$$n(r, z) = n_0(r) + \epsilon \sin kz K_0(kr) + \mathcal{O}(\delta^2), \tag{A9}$$

where $K_0(kr)$ is the modified Bessel function; note that

this approaches zero at $r = \infty$, so as long as $b \gg a$, we do not need to consider the boundary condition at b, at least to a first approximation. At the inner boundary, we have

$$n(a + \zeta(z), z) = n_0(a) + \zeta(z) n_0'(a) + \epsilon \sin kz K_0(ka) + \mathcal{O}(\delta^2), \quad \text{(A10)}$$

so that, to first order,

$$\epsilon = -\frac{\delta a n_0'(a)}{K_0(ka)}, \quad \text{(A11)}$$

which is positive during sublimation. To evaluate whether or not the perturbation will grow, we now use (A9) to calculate the flux at maxima and minima of R (where the normal to the surface has no z component):

$$\frac{\partial}{\partial r} n|_{r=R} = n_0'(a) + n_0''(a)\zeta(z) + k\epsilon \sin kz K_0'(ka) + \mathcal{O}(\delta^2), \quad \text{(A12)}$$

where the prime denotes differentiation with respect to the argument. Substituting for ϵ and using (A6) and (A8), we obtain

$$\frac{\partial}{\partial r} n|_{r=R} = -\frac{(n_a - n_b)}{a \ln(b/a)} \left[1 - \frac{\zeta(z)}{a} \left\{ 1 + ka \frac{K_0'(ka)}{K_0(ka)} \right\} \right]. \quad \text{(A13)}$$

This gradient in number density drives the flux and is negative during sublimation. Since thin regions have a negative value of $\zeta(z)$, it is clear that if the quantity in curly brackets in (A13) is positive, then the perturbation will grow. Thus our condition for growing modes is

$$1 + ka \frac{K_0'(ka)}{K_0(ka)} > 0. \quad \text{(A14)}$$

This condition is equivalent to

$$ka < 0.59 \quad \text{(A15)}$$

or

$$\lambda > 10.6 \times a, \quad \text{(A16)}$$

where $\lambda = 2\pi/k$ is the wavelength of the perturbation. We therefore predict that only cylinders of large aspect ratio (greater than 10) will develop necks that sublimate at an enhanced rate, starting from an infinitesimal perturbation. We have observed sublimation of particles for which the initial condition included a "waist" section but whose aspect ratios have not been large enough to accommodate (A16). We saw that the thin region may sublimate away causing the particle to break up, but we did not see enhanced sublimation rates due to thinning.

To test our model, we performed some computer simulations of vapor fields in the vicinity of peanut-shaped particles and found no enhancement of number-density gradients at the neck for aspect ratios less than 10 and moderate perturbations in radius. Physically, we can interpret the result in terms of shadowing: For short-wavelength perturbations, the thicker regions on either side of the thin section control the vapor density in the vicinity of the cylinder, and thus the number-density gradient at the surface is less over the thin region since the distance to the boundary is greater.

Acknowledgments. This work was supported by NSF grant ATM 9528049, by a grant from the Leonard X. Bosack and Bette M. Kruger Charitable Foundation, and by a grant from the University of Washington Royalty Research Foundation. The authors would like to thank D. Hegg and J. Reid of the Atmospheric Sciences Department at the University of Washington for the ion chromatography work and C. Raymond, J. Dempsey, and J. Latham for helpful comments.

References

Andrews, M., Equilibrium charge-density on a conducting needle, *Am. J. Phys., 65*, 846–850, 1997.

Baker, M.B., R. Breidenthal, T. Choularton, and J. Latham, The effects of turbulent mixing in clouds, *J. Atmos. Sci., 41*, 299–304 1984.

Bartlett, J.T., A.P. van de Heuval, and B.J. Mason, The growth of ice crystals in an electric field, *Z. Angew. Math. Phys., 14*, 599–610, 1963.

Blyth, A., and J. Latham, Development of ice and precipitation in New Mexican summertime cumulus clouds, *Q. J. R. Mctcorol. Soc., 119*, 91–121, 1993.

Blyth, A., and J. Latham, A multi-thermal model of cumulus glaciation via the Hallett-Mossop process, *Q. J. R. Meteorol. Soc., 123*, 1185–1198, 1997.

Bower, N.B., S.J. Moss, D.W. Johnson, T.W. Choularton, J. Latham, P.R.A. Brown, A.M. Blyth, and J. Cardwell, A parametrization of the ice water content observed in frontal and convective clouds, *Q. J. R. Meteorol. Soc., 122*, 1815–1844, 1996.

Crowther, A.G., and C.P.R. Saunders, Ice crystal growth in electric fields, *J. Meteorol. Soc. Jpn., 51*, 318–324, 1973.

Dempsey, J.P., Scale effects on the fracture of ice, in The Johannes Weertman Symposium, edited by R.J. Arsenault et al., The Miner., Metals, and Mater. Soc., pp. 351–361, Warrendale, Pa., 1996.

Dong, Y., R.G. Oraltay, and J. Hallett, Ice particle generation during evaporation, *Atmos. Res., 32*, 45–53, 1994.

Glen, J.W., and M.F. Perutz, The growth and deformation of ice crystals, *J. Glaciol. 2*, 397–403, 1954.

Griffiths, A.A., The phenomena of rupture and flow in solids, *Phil. Trans. R. Soc. London, A, Ser. 221*, 163, 1920.

Griggs, D.J., and T.W. Choularton, A laboratory study of secondary ice particle production by the fragmentation of rime and vapour-grown ice crystals, *Q. J. R. Meteorol. Soc., 112*, 149–163, 1986.

Hallett, J., and S.C. Mossop, Production of secondary ice particles during the riming process, *Nature, 249*, 26–28, 1974.

Harris-Hobbs, R., and W.A. Cooper, Field evidence supporting quantitative predictions of secondary ice particle production rates, *J. Atmos. Sci., 44*, 1071–1082, 1987.

Hobbs, P.V., *Ice Physics*, Clarendon, Oxford, England, 1974

Hobbs, P.V., and A.J. Alkezweeny, The fragmentation of freezing water drops in free fall, *J. Atmos. Sci., 25*, 881–888, 1968.

Hobbs, P.V., and A. Rangno, Rapid development of high ice

particle concentrations in small polar maritime cumuliform clouds, *J. Atmos. Sci., 47*, 2710–2722, 1990.

Inglis, C.E., Stresses in a plate due to the presence of cracks and sharp corners, *Trans. Inst. Nav. Archit., 55*, 219, 1913.

Jackson, J.D., *Classical Electrodynamics*, 2 ed., pp. 149–151, John Wiley, New York, 1975.

Jayaratne, E. R., S.-L. Peck, and C. Saunders, Comment on "A laboratory study of static charging by fracture in ice growing by riming" by E.E. Avila and G.M. Caranti, *J. Geophys. Res., 101*, 9533–9535, 1996.

Jayaweera, K.O.L.F., and R.E. Cottis, Fall velocities of plate-like and columnar ice crystals, *Q. J. R. Meteorol. Soc., 95*, 703–709, 1969.

Jellinek, H.H.G., The influence of imperfections on the strength of ice, *Proc. Phys. Soc., 71*, 797–814, 1958.

Lawn, B.R., *Fracture of Brittle Solids* Cambridge Univ. Press, New York, 1975.

Mossop, S.C., Some factors governing ice particle multiplication in cumulus clouds, *J. Atmos. Sci., 35*, 2033–2037, 1978.

Mossop, S.C., The mechanism of ice splinter production during riming, *Geophys. Res. Lett., 7*, 167–169, 1980.

Nakamura, T., and S.J. Jones, Mechanical properties of impure ice crystals, in *Physics and Chemistry of Ice*, edited by E. Whalley et al., pp. 365–369, R. Soc. Can., Ottawa, 1973.

Oraltay, R.G., and J. Hallett, Evaporation and melting of ice crystals: A laboratory study, *Atmos. Res., 24*, 169–189, 1989.

Pruppacher, H.R., and J.D. Klett, *The Microphysics of Clouds and Precipitation*, pp. 450–458, D. Reidel, Norwell, Mass., 1978.

Rangno, A., and P.V. Hobbs, Ice particle concentration and precipitation development in small polar maritime cumuliform clouds, *Q. J. R. Meteorol. Soc., 117*, 207–243, 1991.

Readings, C.J., and J.T. Bartlett, Slip in single crystals of ice, *J. Glaciol., 7*, 479–491, 1968.

Rydock, J.P., and E.R. Williams, Charge separation associated with frost growth, *Q. J. R. Meteorol. Soc., 117*, 409–420, 1991.

Saunders, C.P.R., M. Hickson, M.D. Malone, and J. von Richtofen, Charge separation during the fragmentation of rime and frost, *Atmos. Res., 29*, 261–270, 1993.

Schaeffer, V.J., and R.J. Cheng, The production of ice crystal fragments by sublimation and electrification, *J. Rech. Atmos., 5*, 5–10, 1971.

Steinemann, S., Results of preliminary experiments on the plasticity of ice experiments, *J. Glaciol., 2*, 404–412, 1954.

Swanson, B.D., N.J. Bacon, E.J. Davis, and M.B. Baker, 1998, Electrodynamic trapping and manipulation of ice crystals, *Q. J. R. Meteorol. Soc.*, in press.

Warneck, P., *Chemistry of the Natural Atmosphere*, p.405, Academic, San Diego, Calif., 1988.

N. J. Bacon, Physics Program, University of Washington, Box 351560, Seattle, WA 98195-1560. (e-mail: neilb@geophys.washington.edu)

M. B. Baker and B. D. Swanson, Geophysics Program, University of Washington, Box 351650, Seattle, WA 98195-1650. (e-mail: marcia@geophys.washington.edu; brian@geophys.washington.edu)

E. J. Davis, Department of Chemical Engineering, University of Washington, Box 351750, Seattle, WA 98195-1750. (e-mail: davis@cheme.washington.edu)

(Received September 3, 1997; revised March 18, 1998; accepted March 24, 1998.)